ISPRS Journal of Photogrammetry and Remote Sensing 66 (2011) 597–607

Contents lists available at ScienceDirect

ISPRS Journal of Photogrammetry and Remote Sensing

journal homepage: www.elsevier.com/locate/isprsjprs

Forest parameter estimation in the Pol-InSAR context employing the multiplicative–additive speckle noise model

Carlos López-Martínez [a,*], Xavier Fàbregas [a], Luca Pipia [b]

[a] Universitat Politècnica de Catalunya (UPC), Signal Theory and Communications Department (TSC), Remote Sensing Lab. (RSLab), E-08034 Barcelona, Spain
[b] Institut Cartogràfic de Catalunya, Barcelona, Spain

ARTICLE INFO

Article history:
Received 9 July 2009
Received in revised form 26 March 2011
Accepted 30 March 2011
Available online 22 April 2011

Keywords:
Synthetic aperture radar
Polarimetric interferometry
Polarimetry
Coherence
Speckle

ABSTRACT

This paper addresses the problem of speckle noise on single baseline polarimetric SAR interferometry (Pol-InSAR) on the basis of the multiplicative–additive speckle noise model. Considering this speckle noise model, a novel filtering technique is defined and studied in terms of simulated and experimental Pol-InSAR data. As demonstrated, the use of the multiplicative–additive speckle noise model does not lead to a corruption of the useful information but to an improvement of its estimation. The performance of the algorithm is analyzed in terms of the physical parameters retrieved from the filtered data, that in this work correspond to the forest height and the ground phase. In case of experimental data, the retrieved forest height is compared and validated against Lidar ground truth measurements.

1. Introduction

The most prominent advantage of radar polarimetry is the possibility to synthesize the received power for any polarization basis from its measure in a single basis (Van Zyl et al., 1987). This property was extended in Cloude and Papathanassiou (1998), in the frame of polarimetric SAR interferometry (Pol-InSAR), to improve the quality of an interferogram by maximizing coherence in the polarization space. This idea was considered later on in Papathanassiou and Cloude (2001), Cloude and Papathanassiou (2003), Ballester-Berman et al. (2005) and Lopez-Sanchez et al. (2007) in order to explore the complete space of interferometric coherence as a function of polarimetry, based on the use of coherent scattering models, demonstrating the capability to perform accurate quantitative remote sensing.

The coherent nature of SAR systems lets data be affected by speckle. Despite speckle appearing as a consequence of the scattering process, the complexity of this process, especially in case of distributed scatterers, makes necessary to consider it as a noise component. Hence, from a stochastic point of view the information of interest refers to the different moments that characterize the data probability density function (pdf). In case of one-dimensional SAR systems, the information of interest consists of the image intensity, whereas for multidimensional SAR systems, it refers to the coherency matrix, or to the equivalent covariance or Müller matrices. The importance speckle noise filtering has for a reliable extraction of physical information from SAR data has to be considered from two different points of view: its characterization and its filtering.

Multidimensional homogeneous SAR data are characterized by the multidimensional, zero-mean, complex Gaussian pdf. Though this model fails to characterize more complex situations, as for instance, presence of texture (D'Hondt et al., 2007; Grandi et al., 2003), this model presents a good compromise to describe data in a sufficiently accurate way with a relative mathematical simplicity. Under this hypothesis, it has been demonstrated that speckle results from the combination of multiplicative and complex additive noise sources (López-Martínez and Fàbregas, 2003). The estimation of information, that is, speckle noise filtering, still remains an open question in multidimensional SAR imagery, which complexity increases with the dimensionality of the data. Preliminary alternatives focused on Pol-InSAR filtering have only considered the estimation of the particular complex correlation coefficients (Vasile et al., 2004). Complete Pol-InSAR data filtering has also been conducted (Lee et al., 2003; Foucher et al., 2006; Vasile et al., 2006), but without considering its effect on the quantitative estimation of physical parameters.

The objective of this work is to present and to validate a new alternative to filter speckle noise in Pol-InSAR data, based on the multiplicative–additive speckle noise model (López-Martínez and Fàbregas, 2003). In López-Martínez and Fàbregas (2008) it was already demonstrated that the use of this model improves the filtering process in case of polarimetric SAR data. As it will be shown, the use of the previous speckle noise models results in an improved quantitative estimation of bio- and geophysical

* Corresponding author. Tel.: +34 93 401 67 85.
E-mail address: carlos.lopez@tsc.upc.edu (C. López-Martínez).

0924-2716/$ - see front matter © 2011 International Society for Photogrammetry and Remote Sensing, Inc. (ISPRS). Published by Elsevier B.V. All rights reserved.
doi:10.1016/j.isprsjprs.2011.03.006

parameters when compared with the results obtained when multilook (MLT) filtering is considered. In addition, the analysis conducted in this work allows to obtain a statistical characterization of the forest height and the ground topography parameters, when estimated from Pol-InSAR data based on the random volume over ground (RVoG) scattering model. Thus, the paper is structured as follows. Section 2 lays the foundations of Pol-InSAR and introduces a novel algorithm for Pol-InSAR data filtering. In Section 3, Section 3.1 evaluates this algorithm regarding the forest parameter retrieval process based on simulated Pol-InSAR data. The evaluation continues in Section 3.2, where experimental Pol-InSAR data are employed. The conclusions are detailed in Section 4.

2. Polarimetric SAR interferometry

An interferometric SAR (InSAR) system acquires two SAR images S_1 and S_2 from slightly different positions in space, separated by a baseline B. Before generating the complex interferogram, i.e., $S_1S_2^*$, it is necessary to co-register both SAR images and to range filter the non-common parts of the spectra, in case of distributed scattering, in order to increase coherence (Gatelli et al., 1994). Then, the interferometric complex coherence is defined as

$$\rho = |\rho| e^{j\phi_x} = \frac{E\{S_1 S_2^*\}}{\sqrt{E\{|S_1|^2\}E\{|S_2|^2\}}} \tag{1}$$

where $E\{\cdot\}$ is the expectation value and $|\cdot|$ represents the absolute value. Due to the space diversity, the phase of the interferogram $S_1S_2^*$, i.e., $\phi = arg\{S_1S_2^*\}$, contains both range and topography-dependent information (Bamler and Hartl, 1998). Its accuracy depends on the interferometric coherence, i.e., $|\rho|$, which ranges between zero and one. A value of $|\rho| = 0$ indicates that ϕ contains no information, whereas $|\rho| = 1$ implies that the topographic information contained in ϕ can be estimated without error. Consequently, ϕ_x needs to be estimated in order to retrieve the topographic information, that is, speckle noise must be filtered out in the interferogram.

A Pol-InSAR system works on the basis of acquiring two fully polarimetric data sets from slightly different positions in space. Separately, both data sets are characterized in the same way as a classical PolSAR data set (Cloude and Pottier, 1996). In terms of information content, nevertheless, both may present differences as a consequence of the existing baseline. Collectively, the characterization of the higher dimensional Pol-InSAR data is performed by a natural extension of the characterization of the lower dimensional PolSAR data. However, with respect to the information content, the Pol-InSAR data contains both polarimetric sources of information, the interferometric information and the data necessary to obtain interferometric information as a function of polarization. The individual polarimetric data, in the monostatic case, may be expressed vectorially by means of the target vector (Cloude and Pottier, 1996)

$$\mathbf{k} = [S_{hh}, \sqrt{2}S_{hv}, S_{vv}]^T \tag{2}$$

where ^{T} represents the vector transposition and $\{h,v\}$ denotes the orthogonal linear polarization basis, where h stands for horizontal polarization whereas v stands for vertical polarization, respectively. Finally, $i = 1,2$ refers to each one of the interferometric data sets. The Pol-InSAR target vector is constructed from the combination of the interferometric vectors $\mathbf{k}_i$ for $i = 1,2$

$$\mathbf{k} = [S_{1,hh}, \sqrt{2}S_{1,hv}, S_{1,vv}, S_{2,hh}, \sqrt{2}S_{2,hv}, S_{2,vv}]^T. \tag{3}$$

In case of deterministic scatterers, $\mathbf{k}$ according to Eq. (3) is a deterministic vector. For distributed scattering, $\mathbf{k}$ is a random vector. In case of homogeneous data, $\mathbf{k}$ is characterized by a six-dimensional, zero-mean, complex Gaussian pdf. Under this hypothesis, the useful Pol-InSAR information are completely characterized by the covariance matrix

$$\mathbf{C} = E\{\mathbf{k}\mathbf{k}^H\} = \begin{bmatrix} \mathbf{C}_{11} & \mathbf{K}_{12} \\ \mathbf{K}_{12}^H & \mathbf{C}_{22} \end{bmatrix} \tag{4}$$

where ^{H} indicates complex transposition. The matrices $\mathbf{C}_{11}$ and $\mathbf{C}_{22}$ correspond to the individual polarimetric covariance matrices of the two passes and $\mathbf{K}_{12}$ is the polarimetric interferometric matrix. As observed in Eq. (4), for distributed scatters, the information of interests acquires sense only from a stochastic point of view. Consequently, this information must be estimated from the data, that is, the speckle noise must be filtered out.

Under the assumption of statistical ergodicity and local stationarity, the expectation in Eq. (4) can be estimated by means of spatial averaging. This spatial averaging, referred to as a multilook filtering, corresponds to the maximum likelihood estimator of the covariance matrix $\mathbf{C}$. The estimated covariance matrix

$$\mathbf{Z} = \langle \mathbf{k}\mathbf{k}^H \rangle = \frac{1}{n}\sum_{q=1}^{n} \mathbf{k}_q \mathbf{k}_q^H \tag{5}$$

is referred to as the sample covariance matrix where $\langle \cdot \rangle$ is the spatial averaging and n indicates the number of looks employed to estimate the matrix. Considering $\mathbf{k}$ to be characterized by a six-dimensional, zero mean, complex Gaussian pdf, the random matrix $\mathbf{Z}$ follows a Wishart pdf (Goodman, 1963; Tough et al., 1995; Lee et al., 1994)

$$p_{\mathbf{Z}}(\mathbf{Z}) = \frac{n^{mn}|\mathbf{Z}|^{n-m}}{|\mathbf{C}|^n \widetilde{\Gamma}_m(n)} \mathrm{etr}(-n\mathbf{C}^{-1}\mathbf{Z}) \tag{6}$$

where $\mathrm{etr}(\mathbf{X})$ is the exponential of the matrix trace and

$$\widetilde{\Gamma}_m(n) = \pi^m \prod_{i=1}^{m} \Gamma(n-i+1). \tag{7}$$

In case of monostatic Pol-InSAR data $m = 6$.

2.1. Forest parameter retrieval

The complex correlation coefficient ρ according to Eq. (1) may present different decorrelation contributions

$$\rho = \rho_{System}\rho_{Temporal}\rho_{Baseline} \tag{8}$$

where ρ_{System} takes into account those decorrelating factors depending on the acquisition and image formation processes and $\rho_{Temporal}$ accounts for decorrelation in situations where both interferometric acquisitions are not acquired simultaneously. The factor $\rho_{Baseline}$, that collects the decorrelation due to the different look angles, may be also split into

$$\rho_{Spatial} = \rho_{Rg}\rho_{Vol}. \tag{9}$$

The real component ρ_{Rg} accounts for the decorrelation introduced by the non-common parts of the range spectra, that if filtered out, makes $\rho_{Rg} = 1$. Finally, the component ρ_{Vol} accounts for the decorrelation caused by different projections of the vertical component of the scatter into the two interferometric datasets. This component is directly related to the vertical scattering distribution of the scatter and, therefore, represents an important source of information about the vertical structure of the target under observation, specially in forest applications.

The complex volume decorrelation contribution ρ_{Vol}, considering a vertical distribution of scatterers $F(z)$, may be obtained, after range spectral filtering, as

$$\rho_{Vol} = e^{jk_z z_0} \frac{\int_0^{h_v} F(z) e^{jk_z z} dz}{\int_0^{h_v} F(z) dz}. \tag{10}$$

The parameter k_z is the effective vertical interferometric wave number, that in the case of repeat-pass interferometry is expressed as

$$k_z = \frac{2k\Delta\theta}{\sin(\theta_0)} \tag{11}$$

where $k = 2\pi/\lambda$, $\Delta\theta$ is the angular baseline and θ_0 is the mean incidence angle. The volume decorrelation according to Eq. (10) depends on a reference height, represented by z_0, and on the height of the vertical layer of scatterers h_v with respect to z_0. The function $F(z)$ contains all the additional information to characterize the volume under analysis. In case of the RVoG model (Papathanassiou and Cloude, 2001; Cloude and Papathanassiou, 2003), that accounts for both the wave extinction process occurring at the natural volume and the effects of the surface beneath the vegetation, $F(z)$ is defined as follows

$$F(z) = m_v(\mathbf{w})e^{\frac{2\sigma}{\sin(\theta_0)}z} + m_g(\mathbf{w})\delta(z - z_0) \tag{12}$$

where $\mathbf{w}$ indicates the polarization state vector and z is in the range $[z_0, z_0 + h_v]$. In the previous expression, σ is the mean wave extinction coefficient and the delta function $\delta(z - z_0)$ represents the phase scattering center at height z_0, accounting for the direct ground and the possible dihedral scattering. The parameters m_v and m_g are the volume and the ground scattering amplitudes, respectively. Inserting Eq. (12) into Eq. (10) results in

$$\rho_{Vol}(\mathbf{w}) = e^{jk_z z_0}\frac{\rho_v + \mu(\mathbf{w})}{1 + \mu(\mathbf{w})}. \tag{13}$$

The product $\phi_0 = k_z z_0$ corresponds to the phase related to the ground topography and $\mu(\mathbf{w})$ represents the ground-to-volume ratio

$$\mu(\mathbf{w}) = \frac{2\sigma}{cos(\theta_0)(e^{2\sigma h_v/cos(\theta_0)} - 1)}\frac{m_g(\mathbf{w})}{m_v(\mathbf{w})}. \tag{14}$$

Finally, ρ_v corresponds to the volume decorrelation in absence of the ground component. As it may be seen in Eq. (13), there is a dependence of the volume decorrelation on the polarization, represented by $\mathbf{w}$. The RVoG predicts a variation of the volume decorrelation with polarization only through the ground-to-volume amplitude ratio, $\mu(\mathbf{w})$, that is, the variation with polarization of coherence is induced by the surface beneath the vegetation. Considering Eqs. (12) and (13) becomes

$$\rho_{Vol}(\mathbf{w}) = e^{j\phi_0}\left(\rho_v + \frac{\mu(\mathbf{w})}{1 + \mu(\mathbf{w})}(1 - \rho_v)\right). \tag{15}$$

If Eq. (15) is considered, it has been demonstrated that $\rho_{Vol}(\mathbf{w})$ describes a line, respect to the polarization $\mathbf{w}$, in the complex plane (Cloude and Papathanassiou, 2003). The region of all possible interferometric coherences has been referred to as the coherence region. The shape and extend of this particular region has been considered by several authors in order to retrieve useful information to characterize the target under observation (Tabb et al., 2002; Neumann et al., 2006).

Given the RVoG model Eq. (13), the goal is to invert this model on Pol-InSAR data according to Eq. (4), in order to retrieve those parameters quantitatively that may characterize the forest under observation, primarily the forest height h_v and the ground topography ϕ_0 (Cloude and Papathanassiou, 2003).

2.2. Speckle noise model in Pol-InSAR data

As indicated in Eq. (5), the six-dimensional covariance matrix must be estimated from data to reduce speckle noise. As a result, the speckle filtering process shall affect the retrieved interferometric coherences, and under the assumption of the RVoG model, the retrieved physical forest parameters. Thus, one of the objectives of this work is to demonstrate that the assumption of the multiplicative–additive speckle noise model helps to improve the quantitative estimation of the physical information.

All the elements of the Pol-InSAR covariance matrix result from the complex Hermitian product of two components of Eq. (3). Hence, a noise model for the sample covariance matrix may be obtained from a generalization of a speckle noise model for the Hermitian product of two SAR images $S_p S_q^*$, where the subscripts p and q take into account both the polarimetric and the interferometric information. Under the Gaussian assumption, $S_p S_q^*$ may be modeled as (López-Martínez and Fàbregas, 2003)

$$S_p S_q^* = \psi\bar{z}_n N_c n_m \exp(j\phi_x) + \psi(|\rho| - N_c\bar{z}_n)\exp(j\phi_x) + \psi(n_{ar} + jn_{ai}) \tag{16}$$

where

$$N_c = \frac{\pi}{4}|\rho|_2 F_1\left(\frac{1}{2}, \frac{1}{2}; 2; |\rho|^2\right) \tag{17}$$

and ${}^2F_1(a, b; c; z)$ is the Gauss hypergeometric function. We redirect to (López-Martínez and Fàbregas, 2003) for a detailed description concerning the parameters of the previous model. The term n_m refers to the speckle noise component presenting a multiplicative noise behavior regarding the information of interest. The term $n_{ar} + jn_{ai}$ represents the complex speckle noise component presenting an additive nature with respect to the information of interest. Eq. (16) expresses that speckle noise for $S_p S_q^*$ results from the combination of multiplicative and complex additive noise components which is determined by the complex correlation coefficient ρ that characterizes $S_p S_q^*$. The model Eq. (16) may be extended to all the elements of the covariance matrix $\mathbf{Z}$. For the diagonal elements, it reduces to the classical multiplicative model for the intensity. For the off-diagonal elements, speckle results from the combination of multiplicative and complex additive noise components.

2.3. Model-based Pol-InSAR filter

Based on the previous multiplicative–additive speckle noise model, a new speckle filtering technique for Pol-InSAR data, referred to as MBPolInSAR filter, for Model Based Pol-InSAR filter, is now introduced. This filter follows the principles introduced in López-Martínez and Fàbregas (2008). As indicated, in the case of the diagonal elements, the model reduces to the multiplicative speckle noise model for the SAR image intensity. Hence, the filtering of these terms may be performed with a filtering technique aiming at reducing multiplicative noise sources. This is not the case for the off-diagonal elements, where speckle results from the combination of multiplicative and complex additive speckle noise sources, which combination is determined by ρ. As a result, the speckle noise filtering process for these elements will be optimized if both noise sources are considered.

The processing of the diagonal elements of the covariance matrix is performed via any of the alternatives presented in the literature that consider multiplicative noise, see Fig. 1. The properties of the filter will determine the final properties of the retrieved data, specially in terms of spatial resolution. In the implementation of the MBPolInSAR filter proposed in this section the diagonal elements will be filtered out with the multilook filter, as its simplicity allows a quantitative evaluation of the filter performance.

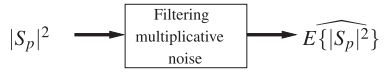

Fig. 1. Processing chain of the MBPolSAR filter for the diagonal elements of $\mathbf{Z}$.

The information contained in the off-diagonal elements of **Z** is affected by multiplicative and complex additive speckle noise sources. The MBPolInSAR filtering approach provides, as a novelty, a procedure to filter both noise sources. Eq. (16) states that the combination of the multiplicative and the additive speckle noise sources is determined by ρ. Since ρ differs among the different off-diagonal elements, the reduction of the multiplicative and the complex additive speckle noise terms must be adapted to each element. Thus, the first step to filter the off-diagonal elements is to estimate ρ. Also in this case, and with the objective to perform a quantitative evaluation of the MBPolInSAR filtering approach properties, a multilook filter with the same averaging level employed to filter the diagonal elements shall be considered. Once estimated, ρ is first transformed to $N_c \exp(\phi_x)$ via Eq. (17), and then the result is multiplied by the single-look amplitude $z = |S_p S_q^*|$. At this point, it is possible to generate the first additive term of Eq. (16). In order to retrieve the correct mean value of $S_p S_q^*$, this product needs to be compensated for parameter B. Given the complex correlation coefficient ρ, previously estimated, B may be straightforwardly estimated via

$$B = \frac{16}{\pi^2}\left({}_2F_1\left(-\frac{1}{2},-\frac{1}{2};1;|\rho|^2\right){}_2F_1\left(\frac{1}{2},\frac{1}{2};2;|\rho|^2\right)\right)^{-1} \tag{18}$$

and applied to generate the product $zN_cB\exp(\phi_x)$. At this stage of the processing chain for a particular element of **Z**, the last step to perform is to filter out the multiplicative speckle noise term n_m with the same approach employed to filter the diagonal elements.

The process presented in the previous paragraph is detailed in Fig. 2. After filtering the multiplicative noise component, an improved estimation of the numerator on the righthand side of Eq. (1) is available. Thus, it is possible to improve the estimation of ρ, that may be employed to filter the complex additive and multiplicative speckle noise components. As shown in Fig. 2, the new value of ρ is reintroduced in the filtering process, making it an iterative process. It is important to highlight that when iterated, filtering is applied to the original non-filtered data, i.e., $S_p S_q^*$. Thus, the original noise model Eq. (16) is valid through the different iterations. The iterative procedure only affects the estimation of ρ, in the way that the better the estimation, the better the separation of the speckle noise components.

3. Results

This section focuses on the quantitative evaluation of the MBPolInSAR filter detailed in Section 2.3 in terms of the statistical properties of the filtered Pol-InSAR data, but primarily in terms of the retrieved forest height h_v and ground phase ϕ_0, when considering the RVoG scattering model. An accurate evaluation of the filtering performance based exclusively on experimental Pol-InSAR data presents severe problems, since it would be practically impossible to uncouple the filtering effects from the possible inaccuracies of the coherent model to fully represent the scattering process. It is also worth noting that when considering h_v and ϕ_0 the determination of the performance of any filtering approach is also affected by the inversion algorithm itself. Nevertheless, if this inversion procedure is constant over the complete evaluation process, one may analyze the effects of the filtering approach on the parameters h_v and ϕ_0.

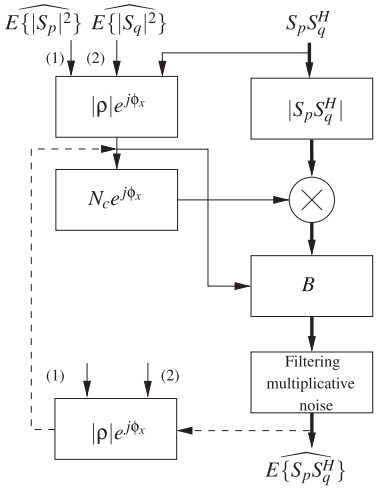

Fig. 2. Processing chain of the MBPolSAR filter for the off-diagonal elements of **Z**.

3.1. Evaluation based on simulated Pol-InSAR data

The simulation of Pol-InSAR data for vegetated areas may be performed using different approaches, under the limitation that this simulation must be coherent in order to make possible the use of the phase information. The simulation considered here consists of a stochastic simulation. As indicated in Section 2, the target vector **k** is distributed according to a multidimensional, zero mean, complex Gaussian pdf. Therefore, a non-correlated **k** vector is first generated, which is subsequently correlated according to the RVoG scattering model, from where h_v and ϕ_0 are inverted (Cloude and Papathanassiou, 2003). Since data are simulated according to the scattering model on which the inversion procedure for h_v and ϕ_0 is based, any deviation of the retrieved information from the nominal or true values may be basically attributed to the speckle noise filtering process. In order to construct **C**, it is also necessary to specify the geometry of the acquisition system. For instance we use parameters of the L-band DLR E-SAR system considering two parallel horizontal tracks, see Table 1. Under this geometry, a particular scenario of a vegetated terrain is assumed, according to the RVoG model. The volume contribution is simulated according to the following coherency matrix

$$\mathbf{T}_v = 0.125\begin{bmatrix}1 & 0 & 0\\ 0 & 0.25 & 0\\ 0 & 0 & 0.25\end{bmatrix} \tag{19}$$

considering a height of $h_v = 20$ m. The ground contribution considers a flat, rough, loamy terrain with 2.2% water content simulated according to the X-Bragg rough surface scattering model (Hajnsek et al., 2003), as specified in Table 2. Both scattering contributions are related with a ground-to-volume ratio of −5 dB. The different Pol-InSAR simulated datasets employed in the following will follow the previous scenario, considering four different horizontal baseline values of 5, 10, 15 and 20 m, with the corresponding k_z parameters of 0.064, 0.129, 0.194 and 0.259 rad/m, respectively.

If one pays attention to Eq. (13), it may be observed that the RVoG model relies on all the information contained within $\mathbf{K}_{12}$. Consequently, it is necessary to determine whether the MBPolInSAR filter, and the multiplicative–additive speckle noise model it is based on, are able, or not, to maintain the information contained in $\mathbf{K}_{12}$, and by extension **C**. Considering the RVoG model, it may be affirmed that maintaining the information contained within **C**, is

Table 1
Flight geometry for simulated Pol-InSAR data.

Range spatial resolution	1.5 m
Azimuth spatial resolution	1.5 m
Wavelength λ	0.23 m
Flight height H	3000 m
Mean incidence angle θ_0	45 deg

Table 2
Parameters of the surface scattering contribution of the RVoG coherent scattering model for simulated Pol-InSAR data according to the X-Bragg model.

Roughness β_1	5 deg
Ground-to-volume ratio μ	−5 dB
Relative permittivity ε_r	3.5
Ground phase ϕ_0	0 deg

equivalent to preserving the nature of the RVoG model, i.e., Eq. (13) describes a line in the complex plane as a function of polarization.

Different works (Tabb et al., 2002; Neumann et al., 2006) have already demonstrated that the first effect of speckle noise on Pol-InSAR data, under the assumption of the RVoG model, is that interferometric coherence does no longer describe a line as a function of polarization, but a region, called coherence region, that is close to the theoretical line. In order to test the MBPolInSAR filter, the set of simulations described before are now considered. Fig. 3 represents the coherent regions corresponding to point samples of the different data sets employed in the simulation, parameterized by B. A first analysis shows that the MBPolInSAR filter preserves the original nature of the data. The effect of the MBPolInSAR filter on high coherence data, i.e., $B = 5$ m, does not differ too much from the results obtained with the standard multilook filter, as the variance associated to the complex additive speckle noise component is negligible. This is not the case as B increases, since more decorrelation is introduced as a consequence of the larger spatial separation. As one may observe, the larger the baseline, the more evident the correction induced by the MBPolInSAR filter as a consequence of the larger importance of the additive speckle noise component.

The following test, detailed in Fig. 4, describes the behavior of the MBPolInSAR filter in terms of the RVoG model, as a function of the dimension of the multilook filter employed to remove the multiplicative speckle noise component and the number of iterations to process the off-diagonal elements of **Z**. This analysis only considers the $B = 15$ m data set, where the coherence regions also correspond to point samples. In all cases, the MBPolInSAR filter is able to retain the information contained in the data without introducing any artifact. As expected, the larger the filter, the higher the reduction of speckle noise. In every case, the coherence regions derived from data filtered with the MBPolInSAR filter considering

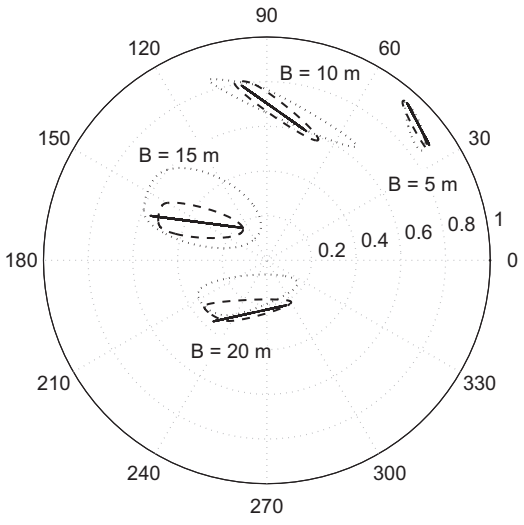

Fig. 3. Coherent regions obtained from simulated data filtered with a 9×9 standard multilook (···) and a 9×9 3 iterations MBPolInSAR (– –) method. Solid lines represent the theoretical variation of coherence with polarization. Angle is expressed in degrees.

one, two and three iterations are also included. The arrows indicate the sense of increasing iterations, in the way that the higher the iterations, the closer the coherence region to the theoretical line.

The qualitative analysis of the coherence regions allows to observe the filtering performances of the MBPolInSAR approach. Nevertheless, a quantitative evaluation in terms of the retrieved coherence regions, is very complex as there is no quantitative way to evaluate and compare the retrieved coherence regions. Therefore, it is necessary to determine how this improvement in the estimation of the coherence regions, with respect to the multilook case, translates into the physical parameters h_v and ϕ_0; and then, to perform a quantitative evaluation of the proposed filtering technique. For this purpose, the inversion algorithm proposed in Cloude and Papathanassiou (2003) to invert forest parameters is considered. These physical parameters correspond to the ground topography ϕ_0 and the forest height h_v. Fig. 5 details the statistical properties of the ground topography ϕ_0, whereas Fig. 6 shows the same analysis, but for the forest height h_v. The evaluation of the information provided by the previous figures must be carefully addressed since these correspond only to the different moments of the pdf of the retrieved values. This information is complemented by the histograms provided by Figs. 7–9.

The first step in the inversion algorithm provided in Cloude and Papathanassiou (2003) is to retrieve the ground phase phi_0 from the crosses of the regression line, obtained from the estimated coherency values, and the unit circle. The ambiguity regarding the ground phase, since the line crosses the unit circle at two points, is broken based on a physical interpretation of the coherency values (Cloude and Papathanassiou, 2003). This ambiguity explains, for instance, the local maximum close to the value $\phi_0 = \pi/2$ rad on Figs. 7 and 8. One may observe that the presence of this maximum disappears, in the case of the multilook filter, as we increase the dimension of the filter. For the MBPolInSAR filter case, and a fixed dimension for the multilook filter, 5×5 pixels in the case of Fig. 8, the local maximum decreases as the number of iterations of the filter is increased. The reduction of this phase ambiguity is a direct consequence of the improvement of the filtering performance. A second important observation on Figs. 7 and 8 is the fact that the distribution of the phase around the main maxima in $\phi_0 = 0$ rad is non symmetric. This asymmetry disappears if the number of looks or the number of iterations in the case of the MBPolInSAR filter are increased. Again, this effect disappears as a result of the improved data filtering process. Retaining these two important observations in mind, one may consider now the analysis of Fig. 5. From the curves corresponding to the mean value, two behaviors are observed. On the one hand, the values of ϕ_0 retrieved from data filtered with the MBPolInSAR approach are better than those obtained with the multilook approach. The analysis of the standard deviation curves supports this conclusion, as the standard deviation decreases as the filtering strength increases. The standard deviation curves also show that the MBPolInSAR filter estimates ϕ_0 with a lower standard deviation than the multilook approach for the same dimensions of the multilook filter. Finally, one may observe that the estimation employing the MBPolInSAR technique, compared with the standard multilook approach, improves with the baseline B since, as mentioned before, the additive speckle noise component increases as a consequence of the larger decorrelation.

As it has been shown, the pdf of the retrieved topographic phase ϕ_0 has a complex form that presents a clear dependence on the speckle filtering process. As it may be concluded, the topographic phase, where speckle is filtered using a Multilook or a MBPolInSAR approach and the inversion process is based on the RVoG scattering model (Cloude and Papathanassiou, 2003), presents an clear asymptotic non-biased behavior. The sense of this bias is more difficult to establish, as overestimated and underestimated results have been observed.

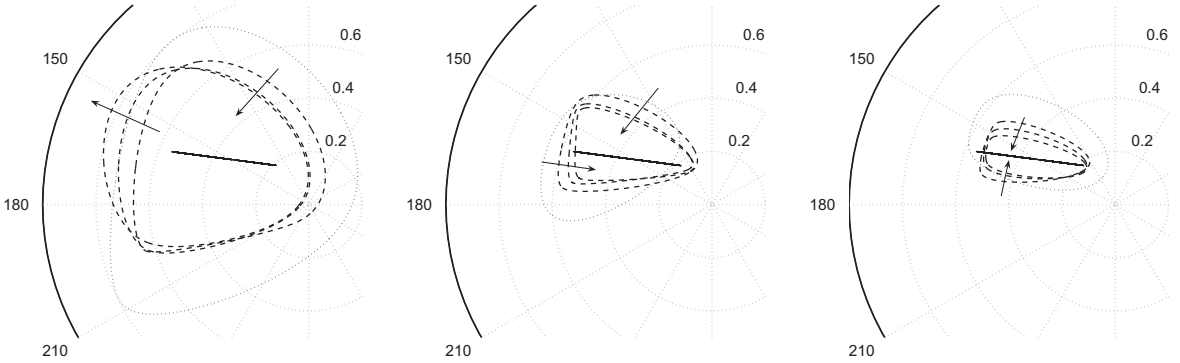

Fig. 4. Coherence regions obtained from simulated data filtered with a standard multilook (···) and the MBPolInSAR approach (– –). In each case, the dimensions of the multilook filter are indicated. The MBPolInSAR filter has been applied with one, two and three iterations. The arrows indicate the sense of movement of the coherence region for increasing scales. Solid lines represent the theoretical variation of coherence with polarization.

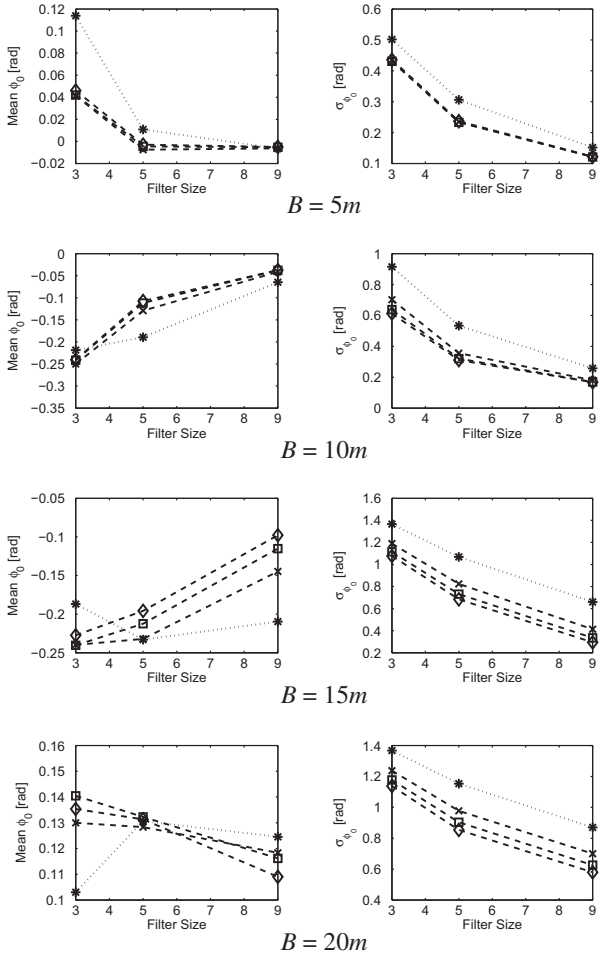

Fig. 5. Mean and standard deviations of the retrieved ground topography for different filtering levels and different baselines. The abscissa axes correspond to the dimension of the multilook filter and the multilook filter within the MBPolInSAR approach to reduce the multiplicative speckle component. Standard multilook (∗), 1 iteration MBPolInSAR (×), 2 iterations MBPolInSAR (□), 3 iterations MBPolInSAR (◇).

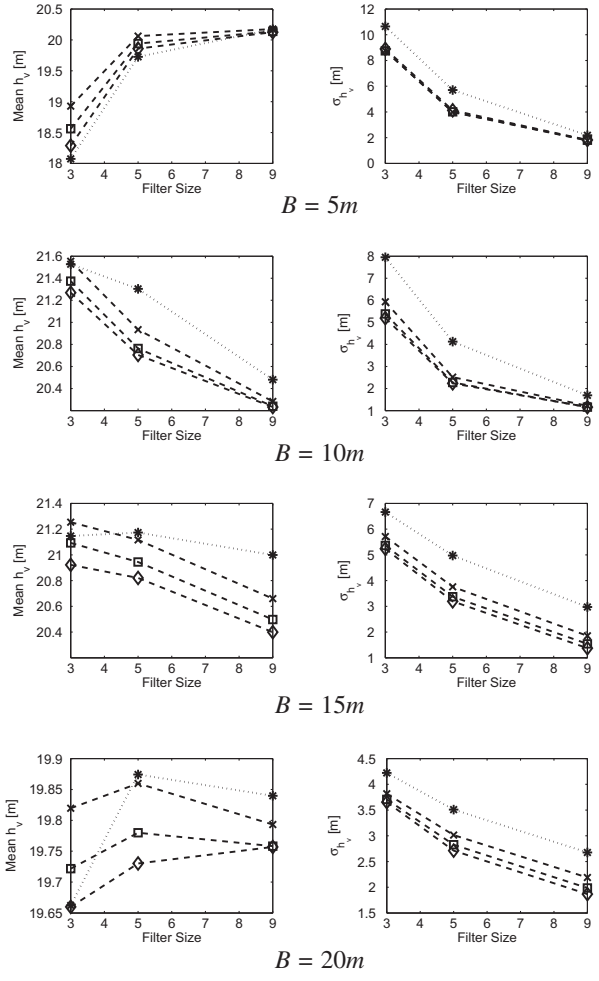

Fig. 6. Mean and standard deviations of the retrieved forest height for different filtering level and different baselines. The abscissa axes correspond to the dimension of the multilook filter and the multilook filter within the MBPolInSAR approach to reduce the multiplicative speckle component. Standard multilook (∗), 1 iteration MBPolInSAR (×), 2 iterations MBPolInSAR (□), 3 iterations MBPolInSAR (◇).

The second step in the inversion algorithm provided in Cloude and Papathanassiou (2003) corresponds to the retrieval of the forest height h_v. Fig. 6 contains the mean and the standard deviation values for the different configurations considered in the paper,

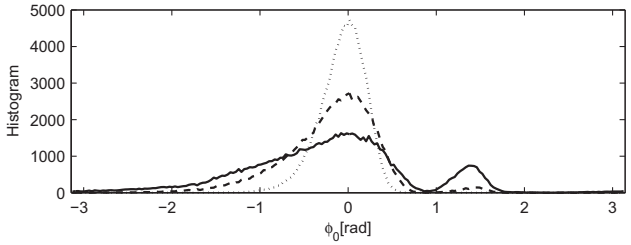

Fig. 7. Retrieved ground topography histograms with simulated data ($B = 10$ m) filtered with 3×3 standard multilook (—), 5×5 standard multilook (– –), 9×9 standard multilook (···).

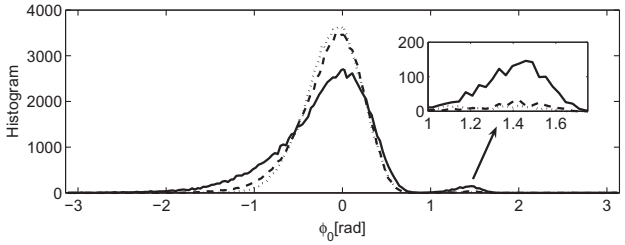

Fig. 8. Retrieved ground topography histograms with simulated data ($B = 10$ m) filtered with 5×5 standard multilook (—), 5×5 1 iteration MBPolInSAR (– –), 5×5 3 iterations MBPolInSAR (···).

whereas Fig. 9 shows the corresponding histograms for some particular configurations. The histograms in Fig. 9 detail a comparison of the height values retrieved from data filtered with a 9×9 multilook and the MBPolInSAR filter employing the same averaging level with one and three iterations. The height values obtained with data filtered with the MBPolInSAR filter are more centered around the theoretical value, i.e., $h_v = 20$ m, than those obtained with the multilook filter. Fig. 9 also demonstrates the effect of the MBPolInSAR filter as a function of B. An increase of the baseline induces more decorrelation in the data, that is, it produces an increase of the standard deviation of the real and imaginary parts of the additive speckle noise component. Consequently, the effect of the MBPolInSAR filter is more evident for large baselines. The shape of the distributions, together with the standard deviation values detailed in Fig. 6, shows the improvement in the height estimation process with data filtered with the MBPolInSAR approach. The reduction in the standard deviation is evident, independently of the multilook filter size within the MBPolInSAR filter to reduce the multiplicative speckle noise component. In addition, the larger the number of iterations, the higher the reduction of the standard deviation. Nevertheless, it is important to notice the disappearance of this bias as the number of samples to reduce the speckle noise is increased. All the previous observations allow to consider now the results detailed in Fig. 6. As one may observe, the MBPolInSAR approach is able to improve the estimation of the forest height by obtaining a mean value closer to the actual one and estimating it with a lower standard deviation for any baseline value, comparing it with an equivalent multilook approach.

In relation with the results found in the case of the topographic phase, the estimation of the forest height, under the same conditions, may also be defined as asymptotically non biased. Also in this case, the different results that have been found do not give enough evidence to determine the sense of this bias and its dependence on the data.

The last aspect that is considered in this section is the capability of the MBPolInSAR filter in order to maintain the spatial resolution. In order to test it, two new data sets with a spatial baseline of 10 m have been generated. The first data set simulates a background forest with a height of 10 m and a small patch with a height of 20 m. The second data set simulates the opposite situation. Data have been processed with a 5×5 multilook filter, a 5×5 multilook filter iterated three times for comparison purposes and the MBPolInSAR approach considering the 5×5 multilook filter and iterated three times. Fig. 10 plots a profile of the retrieved height for every data set, where the patches are theoretically located between pixels 50 and 65. Both profiles show that, despite the iterative nature of the MBPolInSAR filter, the resolution with which forest height is retrieved is close to the one of the standard multilook. It is worth to notice that in the current implementation of the MBPolInSAR filter, spatial resolution maintenance has not been a main issue since the objective is to prove the performance of the filtering approach itself. Obviously, the spatial resolution would be improved if within the MBPolInSAR filter the multilook filter is substituted with an improved filtering technique.

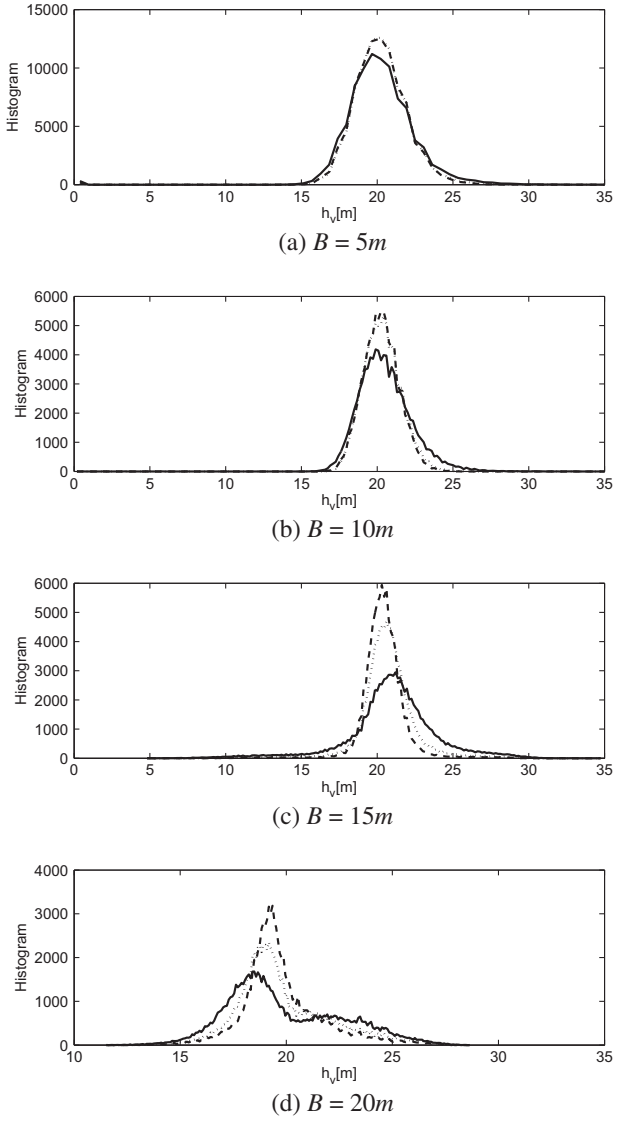

Fig. 9. Retrieved height histograms with simulated data filtered with standard 9×9 multilook (—), 9×9 1 iteration MBPolInSAR (···), 9×9 3 iterations MBPolInSAR (– –).

3.2. Evaluation based on real Pol-InSAR data

The real data employed in this work are part of the second Indonesian Airborne Radar Experiment (INDREX-II), conducted in 2004

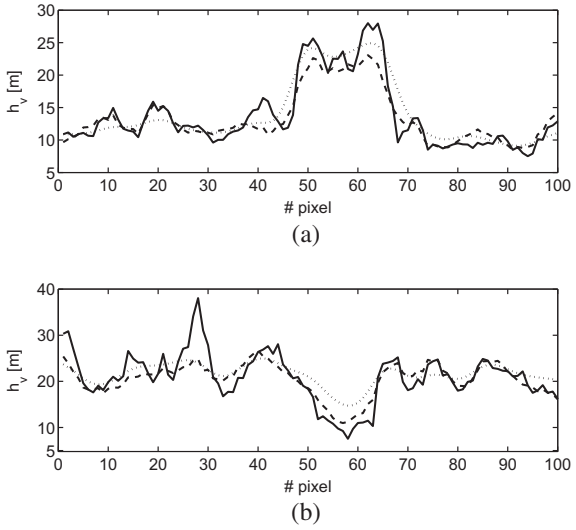

Fig. 10. Spatial resolution properties. (—) 5 × 5 Multilook, (· · ·) 5 × 5 3 it. Multilook, (– –) 5 × 5 3 it. MBPolInSAR.

on the Kalimantan island of Indonesia (Hajnsek et al., 2005). The objective was to conduct an extensive measuring campaign to support the development and validation of quantitative parameter estimation techniques from multidimensional SAR data on tropical and sub-tropical forest regions. The acquisition process was performed with the DLR's experimental airborne SAR system (E-SAR) in November and December of the same year. Additionally, in August 2007, a Lidar measurement campaign was conducted on the same areas imaged in 2004 in the INDREX-II campaign context.

The INDREX-II campaign considered two main test areas that covered the main broad forest types, where data at X-, C-, L- and P-band were acquired. Nevertheless, only a subset of the complete data set acquired in the mission shall be considered. The area considered in this study corresponds to the Mawas test site, located in central Kalimantan, Indonesia. The area presents a relatively flat area covered by a tropical peat swamp forest types where forest height ranges from 15 to 30 m, and biomass levels in the range of 20–250 t/ha. The evaluation of the filtering approach developed previously shall be performed considering three PolSAR acquisitions, making possible to construct two Pol-InSAR data sets with baselines of 15 and 30 m, see Table 3. Fig. 11 shows the Span image of the master image, labeled 1402, that shows the homogeneity of the studied forest.

For the data sets indicated in Table 3, Lidar measurements were performed with a spacial resolution in the range of 2–3 m. The definition of forest height is not unique. In addition, the forest height that may be retrieved from SAR or Lidar data depends, of course, on the morphology of the forest that determines the penetration capabilities of the microwave or the optical radiations. Nevertheless, it has been shown that the forest height retrieved from Pol-InSAR data closely matches the so-called h_{100} height (Mette et al., 2004), that corresponds to the average height of the 100 tallest tress per hectare. Consequently, the raw Lidar data has been processed in order to derive an h_{100} on different segments of the Lidar data set. This measure of h_{100} obtained from Lidar data shall be employed to validate the forest height inverted from experimental Pol-InSAR data. In order to perform this quantitative evaluation, only a 140 range-pixels × 1200 azimuth-pixels area is considered, where SAR and Lidar data are available, see Fig. 11.

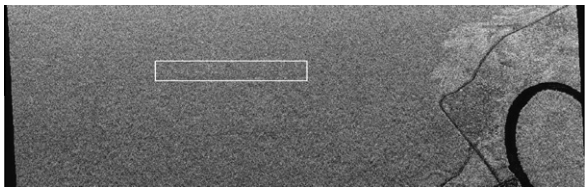

Fig. 11. Span image Indrex-II 1402 dataset. The framed sector corresponds to the area of analysis.

The Pol-InSAR data sets detailed in Table 3 have been processed with a 9 × 9 multilook approach and the MBPolInSAR filter considering also a 9 × 9 multilook filter. In this case, three iterations have been assumed. Fig. 12 presents the retrieved forest height h_v and the ground phase ϕ_0 for the 1402–1405 Pol-InSAR data set, whereas Fig. 13 shows these parameters for the 1402–1408 data set. From a global and qualitative comparison of these results, both filtering approaches result in similar retrieved parameters. Hence, these results allow to establish the important conclusion that the assumption of the multiplicative–additive speckle noise model does not lead to a corruption of the retrieved physical parameters. In order to support this conclusion, and in order to study the implications of the assumption of this speckle noise model, the results in Figs. 12 and 13 are quantitatively analyzed in the following.

From Figs. 12 and 13, the analyzed area may be considered almost homogeneous in terms of forest height and ground phase. Hence, the mean and the standard deviation values may be considered as a first tool to perform a quantitative analysis, see Tables 4 and 5. The mean forest height obtained from data filtered with the MBPolInSAR approach is lower than the mean forest height from data filtered with a multilook filter, which is in accordance with the observations based on simulated SAR data. Thus, it is possible to deduce that the forest height values obtained through the MBPolInSAR approach are closer to the actual values. The standard deviation values also show the same behavior, demonstrating the filtering performance of the MBPolInSAR technique over the multilook approach. The mean and standard deviation values corresponding to ϕ_0 also present the same behavior, allowing also to support the efficiency of the proposed filtering technique.

Lidar measurements are available for the same area, that after a processing step have been transformed into the h_{100} height for different segments. The data considered previously cover approximately 30 segments of the complete Lidar data set. The comparison of the height retrieved from Pol-InSAR data against the Lidar data may be performed into two different ways. The first comparison is a pixel-to-pixel comparison of the retrieved height from Pol-InSAR data with the corresponding pixels of the Lidar data, despite Lidar data represent only h_{100} for different segments. This validation is performed via the histograms of the retrieved heights. These results are depicted in Fig. 14a for the 1402–1405 Pol-InSAR data set, whereas the results for the 1402–1408 data set are in Fig. 15a. The second comparison makes reference to a segment-to-segment comparison, performed through a regression, where for every segment, the h_{100} measure is compared against the mean Pol-InSAR height derived in the same segment. Results are in Fig. 14b and 15b, respectively. These results are complemented with Table 5, where the mean and the standard deviation values of the retrieved forest height, and its difference with the h_{100} Lidar measurements defined as

$$\Delta h_v = h_v - h_{100} \tag{20}$$

Table 3
Indrex II P-band datasets.

Master Img.	Slave Img.	Baseline	k_z range
1402	1405	15 m	0.03–0.13 rad/m
1402	1408	30 m	0.06–0.26 rad/m

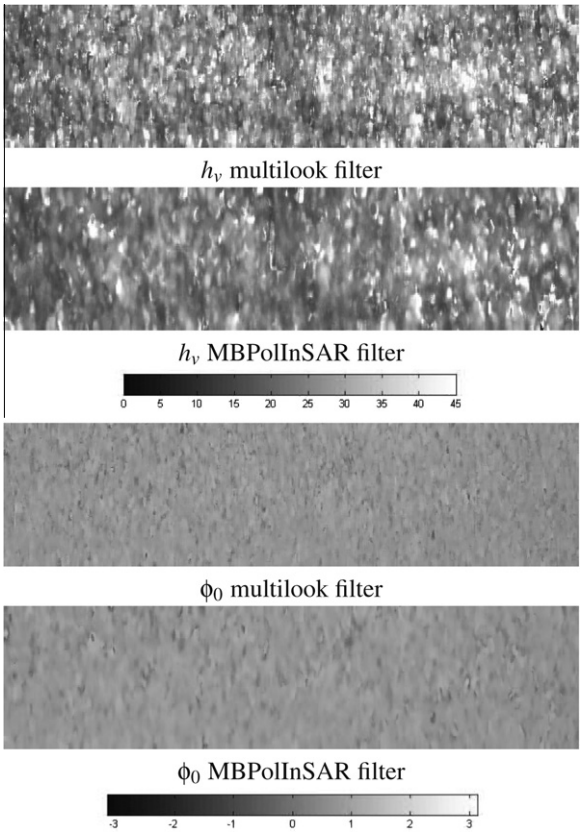

Fig. 12. Retrieved height [m] and ground phase [rad] based on the acquisitions 1402–1405.

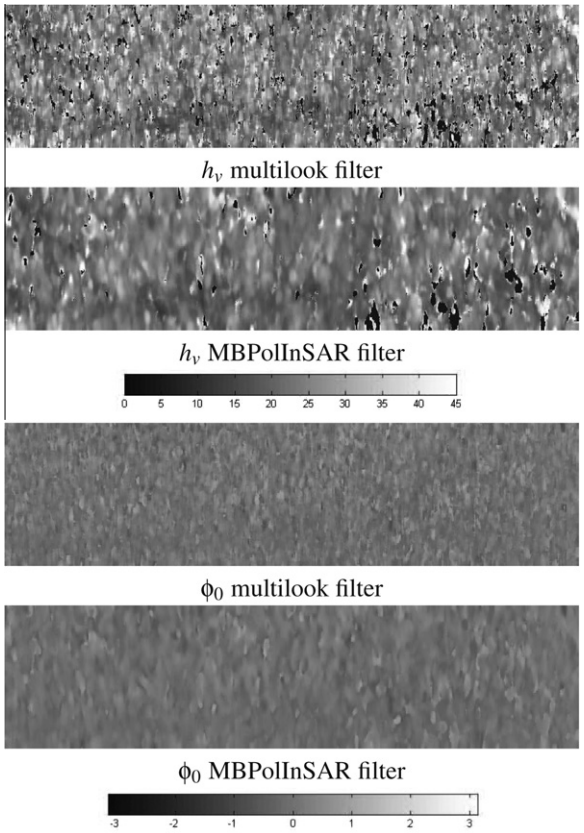

Fig. 13. Retrieved height [m] and ground phase [rad] based on the acquisitions 1402–1408.

for the pixel-to-pixel and segment-to-segment comparisons are presented for both data sets.

The histograms resulting from the pixel-to-pixel comparison of the retrieved height inverted from Pol-InSAR data against the Lidar data show first that the inversion approach proposed in Cloude and Papathanassiou (2003) is able to retrieve the correct forest height. A detailed analysis of the results makes evident that the forest height values retrieved from data filtered with the MBPolInSAR approach are closer to the h_{100} measurements as corroborated in Table 5. As observed for both data sets, the mode of the histograms for data filtered with the MBPolInSAR approach are closer to the Lidar measurements. It is worth to notice that in the case of the MBPolInSAR filter, the retrieved heights tend to be substantially lower than in the case of the multilook approach. This behavior of the height values obtained from data filtered with the MBPolInSAR approach are consequent with the morphology of the forest in the Mawas test site, where heights are in the range of 15–30 m. The second comparison has been performed in terms of the mean height obtained for the 30 segments considered in this work. The Lidar measurements correspond to the h_{100} value for every segment, whereas for the same segment, the mean Pol-InSAR height is computed. Results are reported in Figs. 14b and 15b and Table 5. In the case of the segment-to-segment comparison, the same trends observed previously are obtained. For both data sets, the use of the MBPolInSAR filtering approach results in lower height values for all the segments of the study.

Table 4
Estimated topographic phase statistical evaluation in a pixel-to-pixel basis.

Data set	Param.	Mean		Std. dev.	
		MLT	MBPolInSAR	MLT	MBPolInSAR
1402–1405	ϕ_0 [rad]	0.66	0.69	0.22	0.19
1402–1408	ϕ_0 [rad]	−0.06	−0.12	0.28	0.21

Table 5
Estimated height from Pol-InSAR data compared with Lidar measurements, where px represents the pixel-to-pixel and sg the segment-to-segment comparison, respectively.

Data set	Param.	Mean		Std. dev.	
		MLT	MBPolInSAR	MLT	MBPolInSAR
1402–1405	h_v px [m]	29.88	27.48	9.51	7.76
	Δh_v px [m]	5.68	3.29	9.61	7.90
	h_v sg [m]	29.85	27.49	2.54	2.32
	Δh_v sg [m]	5.65	3.30	2.92	2.81
1402–1408	h_v [m]	27.10	24.97	9.70	7.06
	Δh_v px [m]	2.90	0.77	9.73	7.10
	h_v sg [m]	27.30	25.10	1.42	1.49
	Δh_v sg [m]	3.11	0.90	1.62	1.67

4. Discussions and conclusions

This paper has presented and validated the application of the multiplicative–additive speckle noise model to define a filtering technique on Pol-InSAR data. The particularity of the performance analysis conducted in this work is that the proposed filtering approach has been tested in terms of the quantitative retrieval of physical parameters. From a global perspective point of view, the results demonstrate that to consider the multiplicative–additive speckle noise model to process Pol-InSAR data does not lead to a damage or to a loss of useful information, but it helps to improve

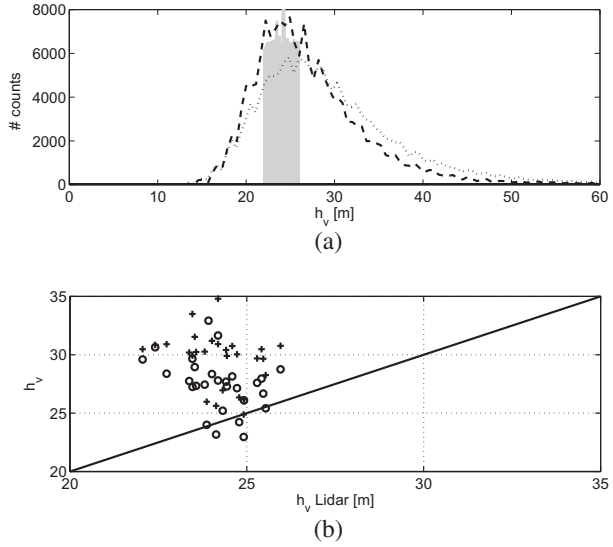

Fig. 14. Validation of Pol-InSAR height for the 1402–1405 dataset. (a) Pixel-to-pixel validation. (···) MLT filter, (– –) MBPolInSAR, Lidar h_{100} is in gray. (b) Segment-to-segment validation. (+) MLT filter, (○) MBPolInSAR.

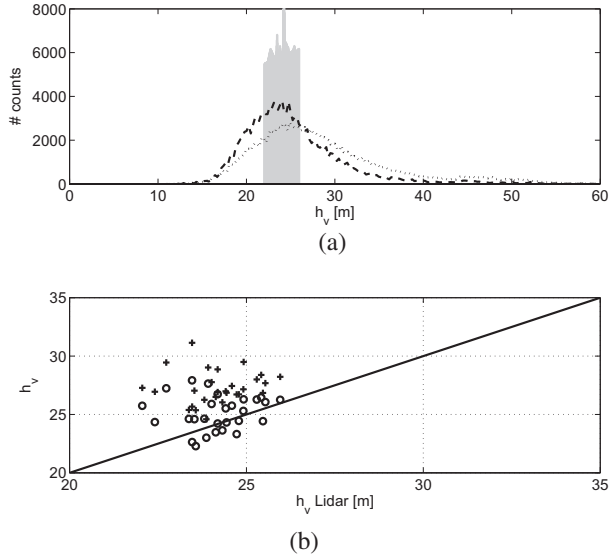

Fig. 15. Validation of Pol-InSAR height for the 1402–1408 dataset. (a) Pixel-to-pixel validation. (···) MLT filter, (– –) MBPolInSAR, Lidar h_{100} is in gray. (b) Segment-to-segment validation. (+) MLT filter, (○) MBPolInSAR.

the estimation process. The key reason of this improvement must be found in the fact that the MBPolInSAR filtering approach considers specifically the additive speckle noise component affecting the off-diagonal elements of the sample covariance matrix. As it is shown in previous works, and also made evident in this paper, to consider this speckle noise component explicitly improves the information estimation process for those areas characterized by low correlation coefficients, as the variance of the additive speckle noise component increases when decreasing the coherence values. Another global conclusion that may be extracted, despite already demonstrated by other authors, is the validity of the use of Pol-InSAR data for the quantitative retrieval of forest parameters based on a coherent modeling.

The use of simulated Pol-InSAR data to evaluate the MBPolInSAR filtering approach and to compare it with the multilook filtering technique has demonstrated that for the same level of spatial averaging, the MBPolInSAR approach outperforms the multilook approach. It has been shown that the forest height and the topographic phase biases, regarding the actual values, are reduced for any measuring condition, together with a reduction of the standard deviation value. This improvement on the forest height estimation increases with the baseline, as coherence decreases with baseline. The previous observations have also been corroborated by considering the use of real P-band Pol-InSAR data, where Lidar measurements have been considered as a ground truth.

The retrieval of the forest height and the topographic phase, as indicated, depends on the process employed to remove speckle noise. But this retrieval process depends also on the electromagnetic inversion process. An estimation process based on multilook or MBPolInSAR approach followed by the inversion process presented in Cloude and Papathanassiou (2003), based on the RVoG coherent scattering model, results in asymptotically non-biased estimations of the forest height and the topographic phase. This conclusion is supported by the analysis of simulated, as well as by the analysis of real Pol-InSAR data and its comparison with Lidar measurements. Finally, an analytical analysis should be necessary to study these effects.

Acknowledgements

The authors would like to thank the Deutsches Zentrum für Luft- und Raumfahrt (DLR) for providing the PolSAR data. This work has been financed by the Spanish Education and Science Ministry through the TEC Project (TEC2007-65690) and the Ramón-y-Cajal Program.

References

Ballester-Berman, J., Lopez-Sanchez, J., Fortuny-Guasch, J., 2005. Retrieval of biophysical parameters of agricultural crops using polarimetric SAR interferometry. IEEE Transactions on Geoscience and Remote Sensing 43 (4), 683–694.

Bamler, R., Hartl, P., 1998. Synthetic aperture radar interferometry. Inverse Problems 14, R1–R54.

Cloude, S., Papathanassiou, K., 1998. Polarimetric SAR interferometry. IEEE Transactions on Geoscience and Remote Sensing 36 (5), 1551–1565.

Cloude, S., Papathanassiou, K., 2003. Three-stage inversion process for polarimetric SAR interferometry. IEE Proceedings Radar, Sonar and Navigation 150 (3), 125–134.

Cloude, S., Pottier, E., 1996. A review of target decomposition theorems in radar polarimetry. IEEE Transactions on Geoscience and Remote Sensing 34 (2), 498–518.

D'Hondt, O., López-Martínez, C., Ferro-Famil, L., Pottier, E., 2007. Quantitative analysis of texture parameter estimation in SAR images. In: International Geoscience and Remote Sensing Symposium IGARSS. Barcelona, Spain, pp. 274–277.

Foucher, S., Farage, G., Benie, G., 2006. Speckle filtering of polsar and polinsar images using trace-based partial differential equations. In: International Geoscience and Remote Sensing Symposium IGARSS, pp. 2545–2548.

Gatelli, F., Guarneri, A., Parizzi, F., Pasquali, P., Prati, C., Rocca, F., 1994. The wavenumber shift in SAR interferometry. IEEE Transactions on Geoscience and Remote Sensing 32 (4), 855–865.

Goodman, N.R., 1963. Statistical analysis based on a certain multivariate complex Gaussian distribution (an introduction). Annals of Mathematical Statistics 34, 152–177.

Grandi, G.D., Lee, J., Schuler, D., Nezry, E., 2003. Texture and speckle statistics in polarimetric SAR synthesized images. IEEE Transactions on Geoscience and Remote Sensing 41 (9), 2070–2088.

Hajnsek, I., Kugler, F., Papathanassiou, K., Horn, R., Scheiber, R., Moreira, A., Hoekman, D., Davidson, M., 2005. Indrex II – indonesian airborne radar experiment campaign over tropical forest in L- and P-band: first results. In: International Geoscience and Remote Sensing Symposium IGARSS, vol. 6, pp. 4335–4338.

Hajnsek, I., Pottier, E., Cloude, S., 2003. Inversion of surface parameters from polarimetric SAR. IEEE Transactions on Geoscience and Remote Sensing 41 (4), 727–744.

Lee, J., Cloude, S., Papathanassiou, K., Grunes, M., Woodhouse, I., 2003. Speckle filtering and coherence estimation of polarimetric SAR interferometry data for forest applications. IEEE Transactions on Geoscience and Remote Sensing 41 (10), 2254–2263.

Lee, J., Hoppel, K., Mango, S., Miller, A., 1994. Intensity and phase statistics of multilook polarimetric and interferometric SAR imagery. IEEE Transactions on Geoscience and Remote Sensing 32 (5), 1017–1028.

López-Martínez, C., Fàbregas, X., 2003. Polarimetric SAR speckle noise model. IEEE Transactions on Geoscience and Remote Sensing 41 (10), 2232–2242.

López-Martínez, C., Fàbregas, X., 2008. Model-based polarimetric SAR speckle filter. IEEE Transactions on Geoscience and Remote Sensing 46 (11), 3894–3907.

Lopez-Sanchez, J., Ballester-Berman, J., Marquez-Moreno, Y., 2007. Model limitations and parameter-estimation methods for agricultural applications of polarimetric SAR interferometry. IEEE Transactions on Geoscience and Remote Sensing 45 (11), 3481–3493.

Mette, T., Papathanassiou, K., Hajnsek, I., 2004. Biomass estimation from polarimetric SAR interferometry over heterogeneous forest terrain. In: International Geoscience and Remote Sensing Symposium IGARSS, vol. 1, pp. 510–514.

Neumann, M., Reigber, A., Ferro-Famil, L., 2006. Polinsar coherence set theory and application. In: European Conference on Synthetic Aperture Radar EUSAR. Dresden, Germany.

Papathanassiou, K., Cloude, S., 2001. Single-baseline polarimetric SAR interferometry. IEEE Transactions on Geoscience and Remote Sensing 39 (11), 2352–2363.

Tabb, M., Orrey, J., Flynn, T., Carande, R., 2002. Phase diversity: a decomposition for vegetation parameter estimation using polarimetric SAR interferometry. In: European Conference on Synthetic Aperture Radar EUSAR, pp. 721–725.

Tough, R.J.A., Blacknell, D., Quegan, S., 1995. A statistical description of polarimetric and interferometric synthetic aperture radar data. Proceedings of the Royal Society A 449, 567–589.

Van Zyl, J.J., Zebker, H.A., Elachi, C., 1987. Imaging radar polarization signatures: theory and applications. Radio Science 22 (4), 529–543.

Vasile, G., Trouve, E., Ciuc, M., Bolon, P., Buzuloiu, V., 2004. Improving coherence estimation for high-resolution polarimetric SAR interferometry. In: International Geoscience and Remote Sensing Symposium IGARSS, vol. 3, pp. 1796–1799.

Vasile, G., Trouve, E., Lee, J., Buzuloiu, V., 2006. Intensity-driven adaptive-neighborhood technique for polarimetric and interferometric SAR parameters estimation. IEEE Transactions on Geoscience and Remote Sensing 44 (6), 1609–1621.